CHAPTER 5

Exergy Analysis of an MHD-GT Combined Power Plant with Partially Ionized Combustion Products

5.1 Introduction

Continuous search for a more reliable, efficient and sustainable alternative energy source have become a priority in energy policies and security across world economies [1]. Thermal systems are required for conversion of available energy to useful and applicable energy forms. Many such systems are still in developmental stages due to insufficient technological knowhow, lack of funding etc. that requires attention for their realization [2]. Development of thermal systems seeks thorough analysis and investigation that plays a crucial role in estimating the overall performance of a thermal plant. Among other renewable energy sources a slightly mixed form is the MHD power in the sense that it utilizes natural resources such as coal, natural gas etc. in an open-cycle mode.

The MHD power technology has gone through various stages of development and its advantages as a power generation system had led to the initiation of National programs on MHD worldwide in various phases [3]. An MHD system allows direct conversion of heat to electricity without the need to transition to intermediate conversion to mechanical energy due to the absence of rotational parts. This has resulted in reaching a very high working temperature range and higher conversion efficiency over the conventional and other non-conventional power generation systems [4]. A prototype of an MHD closed-loop system for electric car propulsion has been developed [5]. MHD force can be used in pumping applications, such as thrusters for ship and spaceship propulsion [6]. The application of MHD in the production of x-rays or ionic beams, in nuclear fusion and plasma flows, has been

appreciated. Recent developments in biomedical and in clinical research applications have used the MHD effects. MRI, magnetic separation, MHD-based micro-pumps, microfluidic networks, stirrers, coolers, etc. as biomedical devices have been developed [7] in recent years.

MHD power generation is a high-temperature application process that can produce partially ionized species. The ionized form of product gases (plasma) can be thermal and non-thermal and not all particles of combustion are in an ionized state in plasma [8]. At higher temperatures the positive ions and electrons are of major interest due to the large entropy contribution to free energy in the translational part of the products and molecular dissociation to ions is higher over electrons production [9]. Higher conversion efficiency in MHD is attributed mainly to the high-temperature phenomenon and the associated plasma state of the combustion products. Investigations on non-premixed flameless oxidation [10] have reported an increase in the net reaction rate and entropy generation with fuel injection at an angle to the combustion chamber. Another 3–D numerical analysis of the non-premixed flameless oxidation using large eddy simulation (LES) – partially stirred reactor (PaSR) models with variation in inlet conditions [11] has found an increase in the maximum flame temperature when there is vertical fuel injection to the combustion chamber. Investigating flameless oxidation characteristics again with the help of LES, it was observed that CO emission increases and NOx emission decreases with increase in inlet Reynolds number (Re) and mass fraction of fuel diluents [12]. Numerical investigation of the Moderate or Intense Low oxygen Dilution (MILD) combustion of a methane-hydrogen gas mixture [13] has been carried out to understand the effects of plasma injection in a combustion chamber. It was found that the presence of methanide (CH_3) in plasma, improves MILD combustion and reduces NO emission

and ignition delay. Studying MILD combustion of methane-hydrogen mixture, subjected to different swirl velocities of hot flows, reduction in both ignition delay and CO emission was observed [14] with the reactive flow extending radially with a reduced length. In the above study, the reaction chemistry was represented by using the GRI-Mech 2.11 mechanism, a mechanism that contains several elementary reactions of a large number of species together with C-H-O reactions.

As far as MHD is concerned, the flow of plasma is governed by certain basic laws and is affected by applied electric and magnetic field forces, which are related to charge and applied fields [15]. Assuming the magneto-fluid (plasma) is electrically neutral and conductive, a stream of ionized gas that flows through a magnetic field generates electricity, is extracted at the electrodes kept at right angles to the flow and magnetic field [16]. From a flow perspective, as described in [17], the mutual interactions between the flow field and electro-magnetic field are usually governed by the Navier-Stokes equation and Maxwell's equations of electro-magnetism.

Incorporation of MHD power system into conventional thermal power plants could improve the power generation capabilities and could also mitigate pollution by reducing the emission of harmful gases [18]. In MHD systems, coal can be used as fuel due to its long-term availability and a nuclear/MHD combination can provide high efficiency. MHD power generation has high efficiency and CO_2 recovery capabilities, higher than other base-load-type fossil power technologies, and could be realized as a predominant topping cycle with the appropriate investigation of its various inherent features [19]. There have been exchanges of technical and scientific data among countries worldwide to tackle issues in the realization of MHD electrical power generation [20]. In an MHD power generation system, power extraction is done through electrodes attached to the walls of a flow duct called the generator. There are

different types of MHD generators such as Faraday linear, Faraday segmented, diagonal, etc. and differences exist between the plasma of combustion products and inert gases [21]. The inlet air to the MHD combustor when preheated using the hot exhaust of the generator enhances plant efficiency; has better chemical recuperation (increasing chemical energy and exergy of fuel) effects and thus helps in fuel-saving [22]. The plasma conductivity can be enhanced by using a fractional amount of suitable seed materials. But deposition of such materials has corrosive effects on air heaters [23]. Increasing seed fraction with respect to electron does not necessarily increase the fluid conductivity. The electrical conductivity is independent of electron temperature when a high seed fraction is considered for high electron temperature in fully ionized seed conditions [24]. The seed material can be best utilized where it can be recovered. Experimental results of available seed regeneration processes suggested the development of their critical components [25].

MHD systems have been analyzed to evaluate their performance under various conditions. The thermal efficiency of the MHD system is found to improve using syngas that has better heat recovery at higher temperature as compared to the use of direct combustion products [26]. Investigation of optimum power extraction in MHD generator using subsonic and supersonic inlet Mach numbers [27] shows the presence of an interaction parameter that influences the terminal voltage drop across the load while using different subsonic inlet Mach numbers. Each of the subsonic inlet Mach numbers possesses a particular critical value of these interaction parameters. Beyond the critical value, choked flow can be observed at the nozzle exit plane. For the supersonic inlets, no such critical interaction parameters or choked flow is observed at the nozzle exit plane. An MHD plant under irreversible conditions generates less entropy in its generator when operated at constant velocity rather than at constant

Mach number [28]. A study on the MHD power cycle assuming maximum power density for constant flow velocity has also resulted in improved thermal efficiency [29]. In such a case the compressor and the generator irreversibility are to be taken into account. Theoretical models that couple MHD systems to gas turbines have been developed to obtain higher power output through an increase in the magnetic field, fluid conductivity, and surface area of electrodes [30]. Assuming constant gas velocity and Mach number while studying the effects of heat transfer on MHD plant performance [31], it was reported that an optimum pressure ratio exists for maximum power and efficiency. The performance of a gas turbine topping cycle is affected by variation in ambient temperature, compression ratio, and turbine inlet temperature (TIT), and maximum exergy destruction is observed for the combustion chamber [32].

The performance of thermal systems is evaluated using the laws of thermodynamics. Energy or the first law analysis alone fails to provide a true scenario of energy utilization [33]. Exergy analysis which is based upon the second law is a better approach as it rightly points out the amount, causes, and location of losses within a system [34]. Thermodynamic inefficiencies in different processes can be better understood by adopting the exergy approach [35]. The exergy of thermodynamic systems changes when there is a lack of mutual stable equilibrium with its surroundings [36] and the exergy method serves as a tool that can be applied in the use of energy resources efficiently. Optimization of exergy analysis through the minimization of entropy generation [37] needs a review of the fundamental concepts of irreversibility or the destruction of exergy.

In this chapter, an exergy-based study is conducted for analysis of a coal-fired MHD topping plant combined with a GT plant considering the effects of the partially ionized product species on the exergetic performance of the combined system. MHD

plants were not analyzed in previous studies considering this aspect. Therefore, the novelty of the present work lies in the determination of the thermodynamic property values of the combustion species in ionic and molecular forms and analysis of the MHD-based combined power plant through the application of the well-known exergy method. The present approach involves the determination of the thermodynamic properties of the partially ionized species and those of the un-dissociated molecular species in the first instance. The property values of these ions and molecules are then applied in the exergy model of the system for evaluation of the performance parameters of the MHD combined system.

5.2. System description

Exergy analysis plays a significant role in evaluating a thermal system's performance. Exergy analysis which requires an overall system analysis applies both mass and energy conservation criteria to the evaluated components and compares its results to exergy values. Exergy measures the energy quality and is mostly represented in terms of exergy destruction and exergetic efficiencies. Here, the exergy method is applied on an open cycle MHD-gas turbine combined plant as shown in Fig 5.1. The system is considered for analysis together with other downstream components namely the air heaters, seed recovery unit, desulfurization unit, two process heaters, and the stack. The open-cycle MHD power system uses proper seeding of the combustion process of fossil fuels to enhance the conductivity of product gases and lowering of ionization temperature. The ionized products are accelerated through a nozzle imparting a high velocity to the gas which is directed to the generator. This process is assumed to be isentropic and free from the influence of pseudo-shocks. Usually, in compressible flow through a convergent-divergent nozzle at a high Mach number, when the boundary layer separation occurs due to interaction

between a strong normal shock and the boundary layer, shock bifurcation occurs leading to the formation of a number of shocks (shock train) downstream of the bifurcated shock. The presence of shock train is accompanied by flow deceleration from supersonic to subsonic in the interaction region, commonly referred to as pseudo-shock. Although pseudo-shock waves affect the performance and efficiency of a flow device [38], these are beyond the scope of the present work because, in the present study, the system is analyzed from the thermodynamics point of view.

The generator of the MHD is subjected to a strong magnetic field 'B' applied transversely. The applied magnetic field induces an electric field normal to both the direction of flow and 'B' that produces the necessary electric current. The produced current is collected through the electrodes which are attached to the generator walls.

Contrary to an open cycle, a closed cycle MHD system uses a compressed seeded noble gas which is recirculated following a similar process. The MHD generator exhausts are considered to be composed of only the molecular combustion products due to the fact that the ionization temperature no longer exists towards the generator exit. The MHD generator exhaust remains at a higher temperature but below its ionization temperature as such the exhaust heat can be suitably utilized in a heat exchanger such as the air preheater. For the present analysis, coal and methane gas are selected as fuels, with the first for combustion in MHD and the later for the gas-turbine system. The coal-combustion products are in partially ionized state [8] and a proportion of 2:3 is considered here for the dissociated to un-dissociated combustion products.

In the MHD-GT combined system in Fig 5.1, Two axial flow compressors consisting of a single stage (AC-I) and 17 stages (AC-II) and having a pressure ratio of 10.0 each provide the compressed air to the MHD and gas turbine combustors [49]. The isentropic efficiency of the MHD air compressor is taken at 0.86 and a polytropic efficiency of 0.9 for the GT compressor. The exit temperatures of the two compressors are then determined using the isentropic and polytropic efficiency relations. The isentropic efficiency of the GT compressor is found to be 0.864.

Preheating of combustor inlet air is done through two air heaters (APH-I and APH-II) with the same air-side and gas-side pressure drops of 5% and 4% with efficiencies of 0.95 and 0.70 respectively. The exit air temperatures for the air preheaters I and II have been fixed at 1800 K and 853 K respectively depending upon the fuel used in the two combustors as well as the GT inlet temperature of 1550 K. The inlet and exit gas temperatures of the air preheaters are calculated using air and gas side efficiency relations. Assuming constant volume combustion in the MHD and GT combustors, the adiabatic flame temperature is determined.

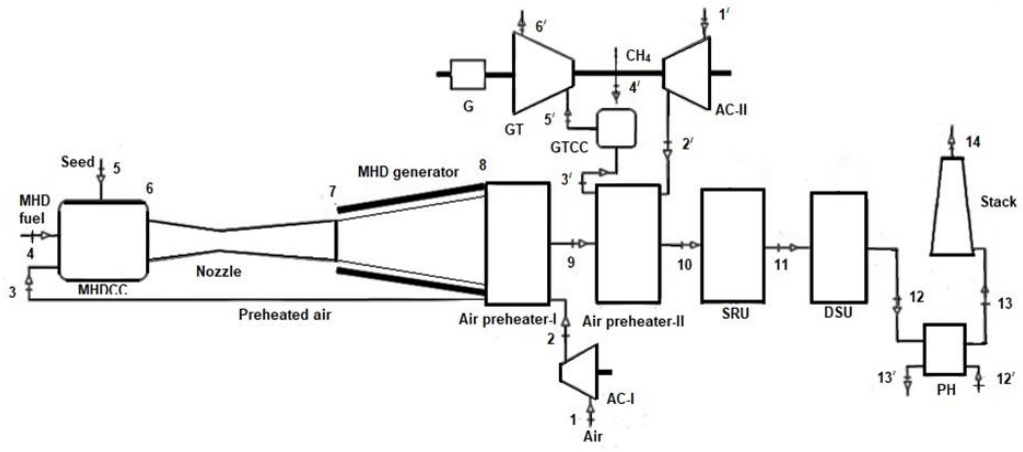

Fig. 5. 1. Schematic of the MHD gas-turbine power plant

5.3 Mathematical modeling

In the MHD system, the combustion stoichiometry considered for the coal and air reaction has been discussed in chapter 3 and 4 respectively, where the variation in coal and air molar compositions (in % wt) is also available. The composition of various types of coal found in different collieries of Assam has been described by [39]. Assuming the total moisture content of coal is equal to the air-dried moisture and using the relations in ASTM D3180/ISO 1170, the mass fraction of the constituents is determined on a DAF basis. Here the air-dried (as determined) part is found to be equal to as-received basis.

5.3.1. Flame temperature

In MHD power generation, since there is a requirement for higher temperature, so constant-volume combustion is assumed during coal combustion. The adiabatic flame temperature (T_{AFT}) for the constant-volume process is obtained by the expression of [40]:

$$H_r - H_p - R_u\left(n_r T_i - n_p T_{AFT}\right) = 0 \tag{5.1}$$

where the product enthalpy is given by

$$H_p = \sum_p n_i \bar{h}_i = \sum_p n_i \left[h_f^0 + \bar{c}_{p,i}(T_{AFT} - T_0)\right] \tag{5.2}$$

and the enthalpy of reaction is given by:

$$H_r = \sum_r n_i \bar{h}_i \tag{5.3}$$

where r, p represents the reactant and products, n is the number of moles. The combustor exit temperature chosen is at a lower value than T_{AFT} obtained.

5.3.2. Combustion of fuel and air

At the high temperature augmented by excess and preheated air, the combustion reaction of coal with air resulted in both molecular and ionic products. Equation (5.4) provides the simple combustion reaction of coal and air as:

$$aC + bH + cO + dN + eS + (0.7751N_2 + 0.2062O_2 + 0.0003CO_2 + 0.0184H_2O)$$

$$\rightarrow$$

$$0.775618N_2 + 0.209O_2 + 0.066225CO_2 + 0.0461H_2O + 0.00155SO_2 \tag{5.4}$$

The reaction mechanism in MHD combustion involves ionized products. At the high ionization temperature, the combustion products are partially dissociated [9] and form ionized species. An estimation of the type of ionic species formation during the high-temperature combustion reaction in MHD can be derived from the reaction mechanism chemistry of [41]. Thus, the overall combustion reaction can be expressed by equation (5.5) as:

$$aC + bH + cO + dN + eS + (0.7751N_2 + 0.2062O_2 + 0.0003CO_2 + 0.0184H_2O)$$
$$\rightarrow [0.775618N_2 + 0.209O_2 + 0.066225CO_2 + 0.0461H_2O + 0.00155SO_2] +$$
$$[0.775618N^+ + 0.209O^+ + 0.066225(C^+ + O^+) + 0.0461(H^+ + OH^+) +$$
$$0.00155(S^+ + O^+)] \quad (5.5)$$

In equations (5.4) and (5.5), coefficients *a, b, c, d, e* represents the percentage mass fractions (in kmol/kg) of coal constituents.

For the partially ionized combustion products, the thermodynamic properties which are dependent on the kind of ionized species and temperature, are calculated, and the electrical conductivity is determined from the known values of the mole fraction, temperature and the momentum collision cross-section with electron [42].

The mass flow rate of air at the states 1, 2, 3 and those at the states $1'$, $2'$, $3'$ are taken as constant assuming constant air properties.

For the MHD, the fuel flow rate is first estimated considering 90% combustion efficiency and conversion efficiency of 0.35 and then the heat rate is calculated in order to obtain the coal flow rate at state 4 for the desired output. For both the plants, the fuel-air ratio has been computed to be 0.074.

5.3.3. Calorific value of fuel

The higher heating value (HHV) for the coal is obtained on a dry and ash-free basis with the elemental composition (% wt) C: 79.11, H: 5.54, S-4.95, O-8.95, N-1.45, A-4.9 (Air-dried), moisture: 2.1, and volatile matter: 45.3. The composition of air based on air molar analysis is N_2: 77.51%, O_2: 20.62%, CO_2: 0.03% *and* H_2O: 1.84%. Combustion calculations for the fuel-air reactions for both MHD and GT combustions are performed to obtain fuel-air ratios with 20% excess air.

In the present analysis, the selected fuel (coal) is from the coalfields found in the state of Assam, India. For solid fuels such as coal the calorific or the HHV is computed using the relation of [43] given in equation (5.6) as:

$$HHV = [152.19H + 98.767]\left[\frac{C}{3} + H - \frac{O-S}{8}\right] \quad (5.6)$$

In equation (6), the letters *C, H, O, N, S* denotes the percentage mass fraction of *carbon*, *hydrogen*, *oxygen*, *nitrogen* and *sulphur* elements present in the coal.

5.3.4. Chemical and physical exergy model

For solid fuel such as the coal, the standard chemical exergy on a DAF basis and the specific chemical exergy of coal considering the ash and moisture content are obtained using the relation of Ref. [33]. In this study, the relations of Ref. [33] using the present coal composition are expressed by the Eqns. (5.7) and (5.8) respectively as:

$$\bar{e}^{ch}_{DAF} = HHV - T_0\begin{bmatrix}\bar{s}_{DAF} + 0.7751\bar{s}_{N_2} + 0.2062\bar{s}_{O_2} + 0.0003\bar{s}_{CO_2} + 0.0184\bar{s}_{H_2O} - 0.775618\bar{s}_{N_2} - \\ 0.209\bar{s}_{O_2} - 0.066225\bar{s}_{CO_2} - 0.0461\bar{s}_{H_2O} - 0.00155\bar{s}_{SO_2}\end{bmatrix} + 0.066225\bar{e}_{CO_2}{}^{ch} + 0.0461\bar{e}_{H_2O}{}^{ch} + 0.00155\bar{e}_{SO_2}{}^{ch} + 0.775618\bar{e}_{N_2}{}^{ch} + 0.209\bar{e}_{O_2}{}^{ch} - 0.7751\bar{e}_{N_2}{}^{ch} - 0.2062\bar{e}_{O_2}{}^{ch} - 0.0003\bar{e}_{CO_2}{}^{ch} - 0.0184\bar{e}_{H_2O}{}^{ch} \quad (5.7)$$

$$\bar{e}^{ch} = 0.93\bar{e}^{ch(DAF)} + \frac{0.021}{18}\bar{e}_{H_2O}{}^{ch}(l) \quad (5.8)$$

For methane, the standard chemical exergy can be obtained using the relation available in [34]. The chemical exergies of the elements can be expressed [33] knowing the standard chemical exergy values of these elements [45]. Accordingly the rates of physical and chemical exergies of the flow streams are computed using relations (5.9) and (5.10) as:

$$\dot{\xi}^{ph} = \left(\bar{h} - \bar{h}_0\right) - T_0(\bar{s} - \bar{s}_0) \quad (5.9)$$

$$\sum x_m \bar{e}_m{}^{ch} + RT_0 \sum x_m ln x_m \quad (5.10)$$

The chemical exergies for the undissociated combustion products given by the above relation remain unchanged at any state of the flow stream so long as the same constituents exist, having the same mole fractions. For the dissociated constituents, the chemical exergies differ from state to state with temperature. The chemical exergy of dissociated gas can be computed based on the standard molar exergies of the components and the Gibbs free energy change at the existing temperatures given by [46] as:

$$\bar{e}_{ion}^{ch} = \bar{e}_{elememt}^{ch} + \Delta\bar{g}_{ion}^{0} - \Delta_f \bar{g}_{element}^{0} \tag{5.11}$$

5.3.5. Molar specific enthalpy and entropy model

The dissociated constituents exist between the MHD combustor and the generator exits, where the products will be in a partially ionized state. In Table 5.1 and Table 5.2, the specific molar enthalpies of the dissociated and undissociated species, are evaluated at the pressures and temperatures of the state points of existence obtained by interpolating the values of the molar specific heats given by the relations in [40] and *JANAF Thermochemical Property Tables*. These relations are given in equations [(5. 12)-(5. 14)]. The computed values of the total specific molar enthalpies are then used to determine the standard molar enthalpies at the given state points. The standard molar enthalpies at a given state point will help in the determination of the energy and exergy rates at that point using the standard relations.

It is taken into consideration that the partially ionized gases exist up to the generator exit to state 8, because the power generation is a result of the ionized gases

$$\bar{h}_i = x\sum x_m \bar{h}_{m,\,dissociated} + (1-x)\sum x_m \bar{h}_{m,\,undissociated} \tag{5.12}$$

$$\bar{s}_i = x\sum x_m \bar{s}_{m,\ dissociated} + (1-x)\sum x_m \bar{s}_{m,\ undissociated} \tag{5.13}$$

$$\bar{s}_{m,\ dissociated/undissociated} = \bar{s}^{0}_{m,dissociated/undissociated} - Rln\frac{x_m p^i}{p^0} \tag{5.14}$$

In equation (5.12), $\bar{h}_m$ is the molar specific enthalpy and x is the fraction of dissociated products. In equations (5.13) and (5.14), $\bar{s}_m$, $\bar{s}_m^0$ are the molar specific entropy and standard molar specific entropies, R is the gas constant, $p^0$and p^i are the

standard and state pressures. In the above three equations, x_m is the mole fraction of product component *m*.

Table 5.1. Molar specific heats and specific molar enthalpies of dissociated MHD combustion product species (kJ/kmol) at the states 6 and 7

State (T_i, p_i)	MHD dissociated products constituents								
	N_2	O_2	CO_2		H_2O		SO_2		$\sum x_m \bar{h}_m$
	$\bar{c}_{p_{N^+}}$	$\bar{c}_{p_{O^+}}$	$\bar{c}_{p_{C^+}}$	$\bar{c}_{p_{O^+}}$	$\bar{c}_{p_{H^+}}$	$\bar{c}_{p_{OH^+}}$	$\bar{c}_{p_{S^+}}$	$\bar{c}_{p_{O^+}}$	
6, 7 (T_0, p_0)	16.508	8.689	1.389	1.377	0.958	1.344	0.032	0.032	9042.592
6 (T_6, p_6)	16.883	4.433	1.377	1.442	0.958	1.869	0.039	0.034	128875.845
7 (T_7, p_7)	16.249	4.346	1.376	1.377	0.958	1.742	0.033	0.032	77795.245

Table 5.2. Molar specific heats and specific molar enthalpies of undissociated MHD combustion product species (kJ/kmol) at the states 6 and 7

State (T_i, p_i)	MHD dissociated products constituents					
	N_2	O_2	CO_2	H_2O	SO_2	$\sum x_m \bar{h}_m$
	$\bar{c}_{p_{N_2}}$	$\bar{c}_{p_{O_2}}$	$\bar{c}_{p_{CO_2}}$	$\bar{c}_{p_{H_2O}}$	$\bar{c}_{p_{SO_2}}$	
6, 7 (T_0, p_0)	22.589	6.139	2.459	3.474	0.062	10352.782
6 (T_6, p_6)	29.343	8.856	4.229	2.726	0.095	215701.649
7 (T_7, p_7)	28.709	8.324	4.119	2.568	0.092	130517.782

Similarly, in Table 5.3 and Table 5.4, the specific molar entropies of the dissociated and undissociated species, are evaluated at the pressures and temperatures of the state points. These values are obtained by interpolating the values of the molar specific heats given by the relations in [40] and *JANAF Thermochemical Property Tables*. These relations are given in equations [(5. 12)-(5. 14)]. Likewise, the computed values of the total specific molar entropies are then used to determine the standard molar entropies at the given state points. Determining the standard molar entropy at a given state point is necessary because these data are required in the exergy rate calculation and without these data, conducting exergy analysis is not possible,

Table 5.3. Specific molar entropies of dissociated MHD combustion product species (kJ/kmol-K) at the state 6 and 7

State (T_i, p_i)	MHD dissociated products constituents								$\sum x_m \bar{s}_m$
	N_2	O_2	CO_2		H_2O		SO_2		
	$\bar{s}_{N^+}$	$\bar{s}_{O^+}$	$\bar{s}_{C^+}$	$\bar{s}_{O^+}$	$\bar{s}_{H^+}$	$\bar{s}_{OH^+}$	$\bar{s}_{S^+}$	$\bar{s}_{O^+}$	
6, 7 (T_0, p_0)	125.580	35.108	11.737	11.757	6.202	9.605	0.337	0.324	200.649
6 (T_6, p_6)	154.635	42.843	14.191	14.208	7.905	12.912	0.396	0.381	247.900
7 (T_7, p_7)	160.005	44.327	15.913	15.926	8.236	12.847	0.406	0.392	258.050

Table 5.4. Specific molar entropies of undissociated MHD combustion product species (kJ/kmol-K) at the states 6 and 7

State (T_i, p_i)	MHD undissociated products constituents					$\sum x_m \bar{s}_m$
	$\bar{s}_{N_2}$	$\bar{s}_{O_2}$	$\bar{s}_{CO_2}$	$\bar{s}_{H_2O}$	$\bar{s}_{SO_2}$	
6,7 (T_0, p_0)	150.255	45.596	15.653	4.404	0.468	216.376
6 $(T_6, p_6$	206.069	61.835	24.191	14.660	0.666	307.422
7 (T_7, p_7)	205.549	59.617	24.597	14.193	0.649	304.605

5.3.6. Energy and exergy model of MHD plant components

The fuel to air ratio for the coal combustion is determined using the basis adjustment factor of 0.93 depending upon the ash and moisture content. Computation of the mass flow rates of air in MHD determines the flow rate for the seeding material, which is 1% of the combined mass flow rates of coal and air. The mass flow rate for the partially ionized combustion products (plasma) of MHD is then determined using the expression given in equation (5.15):

$$\dot{m}_{plasma} = \dot{m}_{seed} + \dot{m}_{air} + \dot{m}_{coal} \tag{5.15}$$

Mathematical modeling of the combined system provides the energy and exergy balance equations at the inlet and exit of each component using standard

energy-exergy models [33]. The exergy model for the combined plant constitutes both energy and exergy balances for the sub-components [34].

For a steady-state-steady-flow (SSSF) process, the mass and energy balances are obtained by the following expressions [(5.16)-(5.17)]:

$$\sum \dot{m}_{in} = \sum \dot{m}_{out} \tag{5.16}$$

$$\dot{Q}_{cv} + \sum \dot{m}_{in}\bar{h}_{in} = \dot{W}_{cv} + \sum \dot{m}_{out}\bar{h}_{out} \tag{5.17}$$

In equation (5.16), $\dot{m}$ is the mass flow rate at a given state. In equation (5.17), $\bar{h}$ is the specific molar enthalpy at the inlet and exit section of a component's control volume (CV), $\dot{Q}_{CV}\ and\ \dot{W}_{CV}$ are the heat and work transfer rates measured within the CV.

The exergy balance is given by:

$$\sum_z (1 - \frac{T_0}{T_z})\dot{Q}_z + \sum \dot{m}_{in}\dot{\varepsilon}_{in} = \dot{\xi}_w + \sum \dot{m}_{out}\dot{\varepsilon}_{out} + \dot{\xi}_D \tag{5.18}$$

In equation (5.18), z is the instantaneous value, $\dot{\varepsilon}$ is the specific exergy rate and $\dot{\xi}_D$ denotes the irreversibility or the exergy destruction rate. The exergy destruction rate is given by the following equation:

$$\dot{\xi}_D = \dot{I}_D = T_0 \dot{S}_{gen} \tag{5.19}$$

The reference environment is chosen to be at temperature $T_0 = 298.15\ K$ and at pressure $p_0 = 1\ bar$. The energy transfer rate $\dot{\Pi}_i$ in MW at any state 'i' of the combined plant is calculated using the following expression:

$$\dot{\Pi}_i = \frac{\dot{m}_i \bar{h}_i}{M_i} \tag{5.20}$$

In equation (5.20), M_i is the molecular weight of the flow stream at state *i*.

The MHD plant consists of two air preheaters for preheating feed air to the combustors of MHD (MHDCC) and GT (GTCC) plant and are positioned after the

MHD generator section to utilize the heat of the high temperature exhaust gases. The MHD generator, a supersonic nozzle, seed recovery unit (SRU), a desulfurization unit and a process heater are other components in the MHD plant with a stack for final release of the gases. The GT plant has a compressor, combustor and turbine as the major components. Both MHD and the GT plant components are evaluated through energy and exergy balance expressions that are given in subsequent sub-sections.

5.3.6.1. Modeling of air compressor

For the air compressor supplying air to the combustor of the MHD, the mass, energy and exergy balances are:

Mass balance: $\dot{m}_1 = \dot{m}_2$

Energy balance: $\dot{I}_2 - \dot{I}_1 = \dot{W}_{AC}$

Exergy balance: $\dot{\xi}_2 - \dot{\xi}_1 = \dot{W}_{cv} - \dot{\xi}_{D,\ AC-I}$

5.3.6.2. MHD combustor energy-exergy model

In the MHD combustor, the inputs supplied are preheated air, fuel, and seed. Thus, the product mass flow rate is the sum of the three input mass flow rates. The mass, energy, and the exergy balance for the MHD combustor are given by the following expressions:

Mass balance: $\dot{m}_6 = \dot{m}_3 + \dot{m}_4 + \dot{m}_5$

Energy balance: $\dot{I}_6 - (\dot{I}_3 + \dot{I}_4 + \dot{I}_5) = \dot{Q}_{CC-MHD}$

Exergy balance: $T_0\dot{S}_{gen} = \dot{\xi}_{D,\ CC-MHD}$

5.3.6.3. Energy-exergy model of the nozzle

The partially ionized products of combustion are imparted with a high velocity by passing them through the nozzle. The nozzle in MHD acts as a gas

accelerator. The mass, energy, and exergy balances for the fluid stream through the nozzle are represented by the expressions given below:

Mass balance: $\dot{m}_6 = \dot{m}_7$

Energy balance: $\dot{I}_6 - \dot{I}_7 = \dot{V}_7 + \dot{I}_{L,\ Nozzle}$

Exergy balance: $\dot{\xi}_6 - \dot{\xi}_7 = \dot{\xi}_{D,\ Nozzle}$

5.3.6.4. Energy-exergy model of the MHD generator

The generator in MHD is a non-conventional component for generating electrical power. The MHD generator receives the high-temperature partially ionized gases to produce power under the influence of the strong magnetic and induced electric field. Nevertheless, the gas velocity, temperature, applied magnetic field, generator size, and type of electrodes matter in the generation of electrical current. Here, the balances for the mass, energy, and the exergy flows can be expressed as:

Mass balance: $\dot{m}_7 = \dot{m}_8$

Energy balance: $\left(\dot{I}_7 + \dot{V}_7\right) - \dot{I}_8 = \dot{W}_{e,gen}$

Exergy balance: $\dot{W}_e = (\dot{\xi}_7 - \dot{\xi}_8) - \dot{\xi}_{D,\ gen}$

5.3.6.5. Air-preheaters energy-exergy model

The air-preheaters receive the high-temperature exhaust gases of the MHD generator to preheat the compressed air streams before entering the combustors. The preheated air helps to raise the combustion temperature. For the air-preheaters, the various balances are given as under:

Mass balance: $\dot{m}_2 = \dot{m}_3$, $\dot{m}_8 = \dot{m}_9$ [for APH-I] and $\dot{m}_{2'} = \dot{m}_{3'}$, $\dot{m}_9 = \dot{m}_{10}$ [for APH-II]

Energy balance: $\left\{\left(\dot{I}_8 + \dot{I}_2\right) = \left(\dot{I}_9 + \dot{I}_3\right)\right\}$ [for APH-I]

and, $\{(\dot{I}_9 + \dot{I}_{2'}) = \left(\dot{I}_{10} + \dot{I}_{3'}\right)\}$ [for APH-II]

Exergy balance: $\left(\dot{\xi}_8 - \dot{\xi}_9\right) - \left(\dot{\xi}_3 - \dot{\xi}_2\right) = \dot{\xi}_{D,\ Aph-I}$ [for APH-I]

and, $\left(\dot{\xi}_9 - \dot{\xi}_{10}\right) - \left(\dot{\xi}_{3'} - \dot{\xi}_{2'}\right) = \dot{\xi}_{D,\ Aph-II}$ [for APH-II]

5.3.6.6. Model for energy –exergy balance of the Seed Recovery Unit

The seed recovery unit or SRU plays an important role in the seed regeneration for reuse, thereby reducing the running cost of the MHD plant. The SRU is also responsible for removing sulphur compounds. In the MHD plant, the mass, energy, and exergy balances for the SRU are given by:

Mass balance: $\dot{m}_9 = \dot{m}_{10} = \dot{m}_{10'}$

Energy balance: $\dot{I}_{10} = \left(\dot{I}_{10'} + \dot{I}_{11}\right)$

Exergy balance: $\dot{\xi}_{10} - \dot{\xi}_{11} = \dot{\xi}_{D,\ SRU}$

5.3.6.7. Model for energy–exergy balance of the Desulphurisation Unit

More sulphur compounds are filtered by the desulphurization unit or DSU, before the gases are passed on to the downstream components or released into the environment. In the MHD system, the DSU receives the gases that are passed through the SRU with the removal of some amount of sulphur compounds. The balances for mass, energy, and the exergy flows in the DSU can be written as given under:

Mass balance: $\dot{m}_{11} = \dot{m}_{11'} = \dot{m}_{12}$

Energy balance: $\dot{I}_{11} = \dot{I}_{11'} + \dot{I}_{12}$

Exergy balance: $\dot{\xi}_{11} - \dot{\xi}_{12} = \dot{\xi}_{D,\ DSU}$

5.3.6.8. Energy–exergy balance of the process heater

The gases exiting from the DSU are at temperature sufficient for the heating application. The process heater acts as a heat exchange device to absorb the heat of the gas stream before it is released into the atmosphere through the stack. The mass, energy, and exergy balances for this device are expressed as given below:

Mass balance: $\dot{m}_{12} = \dot{m}_{13}, \dot{m}_{12'} = \dot{m}_{13'}$

Energy balance: $\dot{I}_{12'} + \dot{I}_{12} = \dot{I}_{13'} + \dot{I}_{13}$

Exergy balance: $\left(\dot{\xi}_{12} - \dot{\xi}_{13}\right) - \left(\dot{\xi}_{13'} - \dot{\xi}_{12'}\right) = \dot{\xi}_{D,PH}$

5.3.6.9. Energy–exergy balance model of the stack

In the MHD plant, the final equipment is the stack. The flue gases exiting to the atmosphere make their way through the stack. The flue gas exiting the stack undergoes a reduction in temperature. For the stack, the balances in mass, energy, and exergy flow streams are given by the following expressions:

Mass balance: $\dot{m}_{13} = \dot{m}_{14}$

Energy balance: $\dot{I}_{13} = \dot{I}_{14}$

Exergy balance: $\dot{\xi}_{13} - \dot{\xi}_{14} = \dot{\xi}_{D,\ Stack}$

5.3.7. Energy and exergy model of GT plant components

As discussed in the previous section, the compressed air to the GT combustor is preheated using the heat of the exhaust combustion gases in the air-preheater-II. The air-preheater for the GT plant receives the hot gases from the air-preheater used in preheating air for the combustor of the MHD plant. Preheating the air in GT improves its efficiency and improves energy savings.

5.3.7.1. Energy and exergy model of the GT air compressor

The air compressor-II is used in the GT plant to compress the air to a high temperature and temperature before it is preheated in the APH-II.

The mass, energy and exergy balances for the air compressor-II can be expressed as:

Mass balance: $\dot{m}_{1'} = \dot{m}_{2'}$

Energy balance: $\dot{I}_{2'} - \dot{I}_{1'} = \dot{W}_{AC}$

Exergy balance: $\dot{\xi}_{2'} - \dot{\xi}_{1'} = \dot{W}_{cv}$

5.3.7.2. Energy and exergy balance model of the GT combustor

The combustion chamber in the GT plant receives pressurized methane fuel and preheated air. The combustion products formed because of the chemical reactions inside the combustion chamber, are used in the turbine located downstream.

The mathematical expressions showing the mass, energy, and exergy balances in the GTCC are given by the following expressions:

Mass balance: $\dot{m}_{5'} = \dot{m}_{3'} + \dot{m}_{4'}$

Energy balance: $\left(\dot{\Pi}_{3'} + \dot{\Pi}_{4'}\right) + \dot{Q}_{in,\ GT} = \dot{\Pi}_{5'}$

Exergy balance: $\dot{\xi}_{3'} + \dot{\xi}_{4'} - \dot{\xi}_{5'} = \dot{\xi}_{D,\ GTCC}$

5.3.7.3. Energy and exergy balance model of the turbine in GT

The combustion gases from the GT combustor is supplied, and expanded in the turbine of the GT plant. Part of the energy so produced is used to drive the GT air compressor. The remaining portion of the energy in the turbine drives the turbine generator to produce electrical energy.

Mathematically, the model balancing for mass, energy and exergy flows in the turbine can be expressed by the following expressions:

Mass balance: $\dot{m}_{5'} = \dot{m}_{6'}$

Energy balance: $\dot{\Pi}_{05'} - \left(\dot{\Pi}_{06'} + \dot{W}_{s,\ GT}\right) = \dot{\Pi}_{L,\ GT}$

Exergy balance: $\dot{W}_{e,\ GT} = \dot{\xi}_{5'} - \dot{\xi}_{6'} - \dot{\xi}_{D,\ GT}$

5.4 Determination of MHD-GT plant performance parameters

While evaluating the performance of the combined MHD-GT system, it's necessary to estimate the values of different related parameters and properties. These include evaluation of energy and exergy rates, exergy destructions in the components, exergetic efficiencies, and the net electrical power output.

5.4.1. Estimation of mass flow rate, temperature and pressure at the state points in the MHD plant

In the present study, the MHD plant has 14 numbers of input streams and 13 numbers of exit flow streams. At each of these input and exit flow stream points, the mass flow rate, pressure, and temperature are evaluated and are listed in Table 5.5. The mass flow rates, pressure, and temperatures at the given state points are evaluated in a similar manner as discussed in section 4.4.2 of chapter 4 with similar assumptions. Similarly, the evaluated values of the mass flow rate, p, T are then used to obtain the energy and exergy rates in the respective state points after the determination of the molar enthalpies and entropies. The energy and exergy rates are used in a similar way to obtain the energy and exergy destructions in the MHD system components and hence evaluate the MHD system performance.

Table 5.5. Mass flow rate, temperature and pressure at various state points of the MHD plant

State	$\dot{m}\ (^{kg}/_{s})$	T (K)	P (bar)	State	$\dot{m}\ (^{kg}/_{s})$	T (K)	P (bar)
1	73.367	298.150	1.000	9	76.535	993.300	1.457
2	73.367	621.000	10.000	10	76.535	731.470	1.385
3	73.367	1800.000	9.500	11	76.535	716.840	1.357
4	2.410	298.150	1.000	12	75.777	702.500	1.289
5	0.758	298.150	20.000	13	75.777	328.106	1.289
6	76.535	4767.000	12.000	12′	144.666	298.150	1.289
7	76.535	2979.000	1.565	13′	144.666	348.150	1.289
8	76.535	2050.000	1.534	14	75.777	308.070	1.000

5.4.2. Calculation of energy and exergy rates of the MHD plant

At a given mass flow rate, the flow streams pass through different state points that exists at some particular pressure and temperature. It is therefore, convenient to estimate the rates of energy and exergies possessed by the flowing streams at those points, and are given in Table 5.6.

Table 5.6. Energy and exergy rates at various state points of the MHD plant in MW

State	$Energy\ rate, \dot{\Pi}(MW)$	$Exergy\ rate, \dot{\xi}(MW)$	State	$Energy\ rate, \dot{\Pi}(MW)$	$Exergy\ rate, \dot{\xi}(MW)$
1	22.631	0.000	9	90.016	36.734
2	48.970	21.549	10	62.692	17.154
3	166.949	112.750	11	61.223	16.056
4	81.147	89.134	12	59.251	13.591
5	0.467	6.095	13	26.926	2.42
6	228.232	205.382	12′	180.558	12.292
7	141.054	105.348	13′	211.273	15.076
8	94.334	64.025	14	25.205	1.448

From the results shown at various state points of the MHD plant in Table 5.6, it is seen that the maximum energy and exergy rates for the MHD plant occur at the state 6 which is the combustor exit while the minimum exergy rate for the MHD plant occurs at the state 14 which is the stack outlet whereas the minimum energy rate is at the state 5 i.e. the seed input point to the combustor.

5.4.3. Determination of exergy flow rates, exergy destruction rate and exergetic efficiency of the components of the MHD plant

As seen from Fig.5.1, each of the 10 components in the MHD plant has input and output exergy flow rates. Thus, the exergy destruction rate in each of these components and their exergetic efficiencies are evaluated as listed in Table 5.7. It can be noted in Table 5.7 that the exergy input to air preheater-I is higher for the obvious reason of computing exergy of undissociated components only beyond the MHD generator.

Table 5.7. Component-wise exergy flow rate, exergy destruction rate and exergetic efficiencies of the MHD plant

Components	$Exergy\ in, \dot{\xi}_{in}(MW)$	$Exergy\ out, \dot{\xi}_{out}(MW)$	$Exergy\ destruction, \dot{\xi}_{D}(MW)$	$Exergetic\ efficiency, \zeta_{II}(\%)$
AC-I	26.339	21.549	4.790	81.823
MHDCC	289.126	205.382	83.744	71.036
Nozzle	100.034	87.178	12.856	87.148
Generator	105.348	87.468	17.880	83.027
Air preheater-I	153.875	149.484	4.391	97.149
Air preheater-II	58.698	52.86	5.838	90.054
SRU	17.154	16.056	1.098	93.599
DSU	16.056	13.591	2.465	84.647
PH	71.543	42.002	29.541	58.709
Stack	2.420	1.448	0.972	59.835

5.4.4. Estimation of mass flow rate, temperature and pressure at the state points in the GT plant

In the GT plant, the number of input and exit flow streams is 7 and 5 respectively. Like in the MHD plant, the mass flow rate, pressure and temperature at each of these input and exit flow stream points are evaluated and are listed in Table 5.8. Using the computed values of mass flow rate, p, and T the energy and exergy rates at al the state points of the GT plant are evaluated. The energy and exergy rates are then used for computing the energy losses and exergy destruction in the GT system components and also in the overall performance evaluation of the GT plant. The highest exergy rate as seen from $\dot{m}$Table 5.8 for the GT plant occurs for the fuel at state $4'$ and that of the energy rate at the GT combustor outlet at state $5'$. The minimum energy and exergy rates are for the air at states $1'$ and $2'$ as shown in Table 5.8.

Table 5.8. Mass flow rate, temperature, pressure, energy and exergy rates at the various state points of the GT plant

State	$\dot{m}\ (kg/s)$	T (K)	P (bar)	$Energy\ rate, \dot{\Pi}(MW)$	$Exergy\ rate, \dot{\xi}(MW)$
$1'$	72.409	298.150	1.000	22.631	0.000
$2'$	72.409	619.260	10.000	48.176	21.964
$3'$	72.409	853.000	9.500	69.858	35.706
$4'$	1.052	298.150	30.000	52.764	107.519
$5'$	73.461	1550.000	9.025	147.547	89.302
$6'$	73.461	975.220	1.040	85.996	26.559

5.4.5. Determination of exergy flow rates, exergy destruction rate and exergetic efficiency of the components of the GT plant

In the GT plant, as shown in Table 5.9, the maximum exergy destruction occurred in the combustor and the minimum in the turbine. It is observed that the turbine is the most efficient component, followed by the air compressor, with the combustor being the least efficient. Compared to the MHD air compressor, as given in Table 5.7, the air compressor of the GT is able to operate more efficiently due to a higher exergy output with comparatively lesser energy input. In Tables 5.7 and 5.9, from a comparison between the generator of the MHD plant and the turbine in the GT plant, it is clear that the turbine is highly efficient with the minimum associated exergy destruction compared to the generator of the MHD plant with correspondingly higher exergy destruction rate. On similar basis, when the two combustors are compared, it is found that although the combustor of MHD is more efficient than the GT combustor, the exergy destruction in the MHD combustor is higher. The reason for these deviations can be accounted to the variations in fuel, temperature and ionization in MHD. The GT plant is also found to have a high overall efficiency in terms of exergy with major exergy destruction in the combustor (GTCC).

Table 5.9. Component-wise exergy flow rate, exergy destruction rate and exergetic efficiencies of the GT plant

Components	$Exergy\ in, \dot{\xi}_{in}(MW)$	$Exergy\ out, \dot{\xi}_{out}(MW)$	$Exergy\ destruction, \dot{\xi}_D(MW)$	$Exergetic\ efficiency, \zeta_{II}(\%)$
Air compressor-II	25.545	21.964	3.581	85.982
GT combustor	143.225	89.302	53.923	62.351
Turbine	62.743	61.551	1.192	98.100

5.4.6. Determination of net power output and exergetic efficiency of the combined MHD-GT

The energy efficiencies of the air compressor and the turbine are evaluated thermodynamically. The compressor has 17 stages with polytropic efficiency of 0.9. The turbine in the present study exhausts into the atmosphere and therefore, the thermodynamic efficiency is obtained from the stagnation temperature difference and stagnation to static pressure ratios [48]. In the present case, the net power output of the combined plant is found to be 59.422 MW with a GT plant output of 36.002 MW and MHD generation of 23.416 MW.

The overall exergetic efficiency for the combined system is 89.23 %. The exergetic efficiency of the MHD plant when computed alone is found to be low about 20% (19.87%). This efficiency is added to the GT exergy efficiency of 69.36% thus obtaining a higher combined efficiency.

5.5. Energy and exergy based performance analyses of the MHD-GT plant

The exergy method in the present work accounts for analyzing MHD power generation by the consideration of partially ionized combustion products which is able to approximate a realistic approach as practical MHD power generation is actually based on ionized gas flows. However, the GT power generation uses the high-temperature MHD waste gases in the molecular state for preheating the reactant air.

5.5.1. Effects of combustion product dissociation on MHD-GT system performance

The energy analysis and the exergy analysis of the MHD system do not provide a real scenario when the combustion products are considered in a molecular state only as could be seen in chapter 4. In Table 5.10, a comparison has been made between the results of exergy destructions and exergetic efficiencies of the MHD components contributing to MHD power. The results are based upon the calculated values for purely molecular and partially ionized combustion products. For the partially ionized products, the values of the exergetic destruction and efficiencies are obtained using the data of Table 5.7 whereas for the undissociated products, these values are evaluated considering the exergy balances of subsection 5.3.6.2 through 5.3.6.4 and utilizing the Tables 5.2 and 5.4 respectively. Thus, from Table 5. 10 a comparison can be drawn on the performance of the MHD system between the two operating conditions.

Table 5.10. Comparison of exergy based results with molecular and with partially ionized combustion products

Component	With molecular combustion products		With partially ionised combustion products	
	$Exergy\ destruction,\ \dot{\xi}_D(MW)$	$Exergetic\ efficiency,\ \zeta_{II}(\%)$	$Exergy\ destruction,\ \dot{\xi}_D(MW)$	$Exergetic\ efficiency,\ \zeta_{II}(\%)$
MHDCC	10.540	96.354	83.744	71.036
Nozzle	55.434	80.101	12.856	87.148
Generator	90.828	90.828	17.880	83.027

From Table 5. 10 it is seen that when the combustion products are in the molecular state, then the MHD generator, nozzle and the combustion chamber are the components in decreasing order of exergy destruction rate. This trend is however not seen when partially ionized combustion products were considered. With partially ionized combustion products, the combustion chamber is the component with highest exergy destruction rate followed by the generator and the nozzle. Further, it is observed that the components with less exergy destruction rate also have a higher

exergy efficiency. Assuming the combustion products are totally in the molecular state, the total rate of exergy destruction in the MHD plant with the three main components is 156.802 MW. However, in the partially ionized state, the total exergy destruction is 114.48 MW. Thus, there is a reduction in the total rate of exergy destruction when the combustion products are in a partially ionized state. Also, the exergetic efficiency of the MHD with the above components shows an improvement of about 21.96 % with the partially ionized combustion products.

5.5.2. Effects of ionization on net power output of MHD-GT system

Although the assumption of purely molecular species in MHD combustion products delivers a higher combined net power output but is highly unrealistic and cannot be achieved in practice because MHD power generation is possible with gas ionization. From section 5.4.6, it is seen that the net power output of the MHD with partially ionized gases is 23.416 MW, thereby delivering a combined power of 59.422 MW. However, with the assumption that MHD power generation is possible with purely molecular species, then the deliverable net power output of the MHD, is found to be 103.762 MW taking the combined MHD-GT power to 136.764 MW which is unlikely with the current method of MHD power generation.

5.5.3. Validation of the results of the present model

The present model has been validated using the GT simulation model of [47] analytically. Though the model of [47] examines both conventional and advanced form of exergy analysis, the validation has been carried out with the conventional results of exergy analysis. Advanced exergy analysis done in Ref. [47] is about splitting the exergy destruction into two parts i.e. avoidable and unavoidable which is beyond the scope of the present study. Therefore, the model was validated by comparing the conventional exergy part of Ref. [47] under identical conditions of pressure, temperature and mass flow rate. The specific heat has been computed as a function of both temperature and mole fraction of constituents and the molar specific

enthalpies of the constituents have been determined. The final form of the combustion reaction from [47] has been expressed as

$$0.09068C_{11}H_{21} + 0.7637N_2 + 0.2054O_2 + 0.03058H_2O + 0.00034819CO_2 \rightarrow$$
$$CO_2 + 1.17157H_2O + 5.47942N_2 \quad (5.21)$$

The molar specific entropies of the constituents have been determined at each station at the given temperature and pressure. The energy rates, exergy rates and the exergy destruction of the flow streams have been computed at each station.

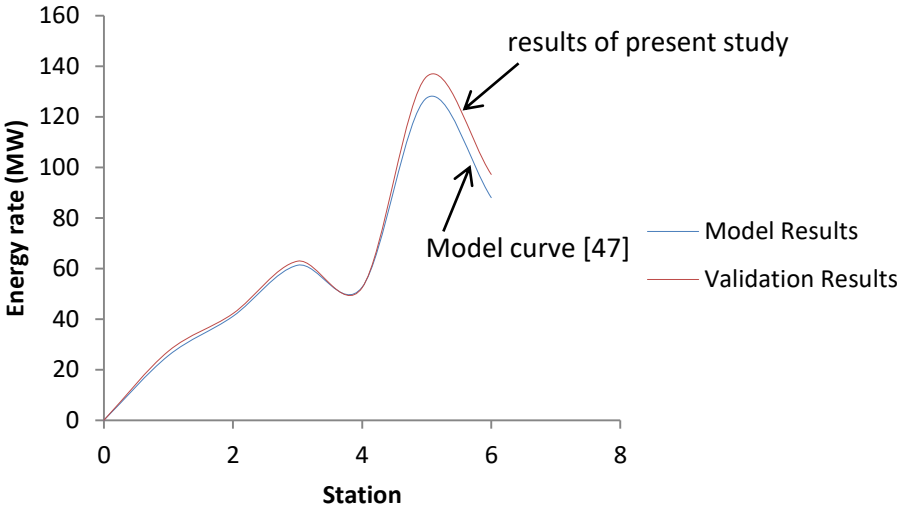

Fig. 5.2. Station-wise energy rates of the gas turbine in *MW*.

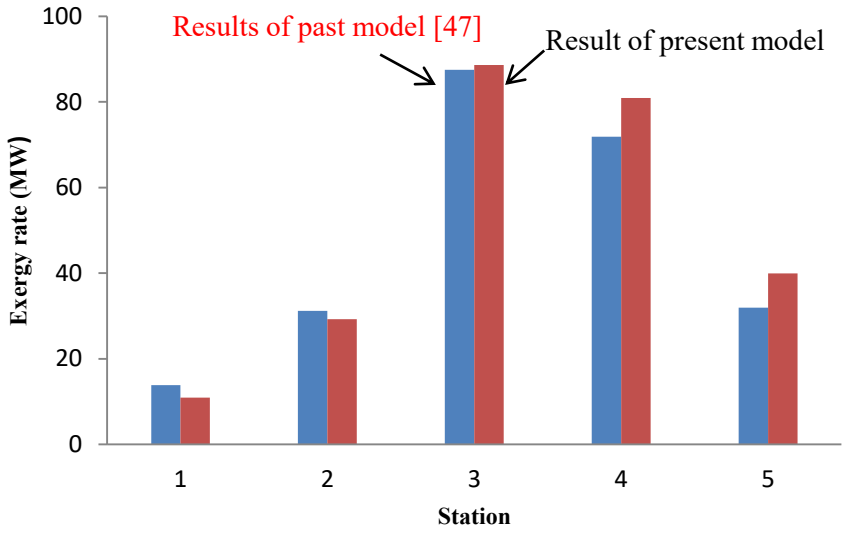

Fig.5.3. Station-wise exergy rates of the gas turbine in *MW*.

The energy and exergy rates from stations 0 to 6 have been determined. The energy and exergy rates in both the present model and the model [47] are zero at station 0 as there is no mass flow rate at this station. The energy rates from station 1 to station 6 increase in both cases as shown in Fig.5.2. The exergy rates, as shown in Fig.5.3, at the stations 0 and 1 are also zero in both cases (Stations 1 to 5 in Fig.5.3 are actually stations 2 to 6) due to zero mass flow rates and use of air at standard reference state with no physical and chemical exergies. The exergy rates increase from stations 2 to 4 and then decrease at stations 5 to 6. Thus, a similar trend is observed in the present model and the model [47]. The results obtained by using the present model are found to be very close to the model values up to station 4 and the deviations are less than 3 units. However, for stations 5 and 6, the energy and exergy rates of the two models show a little departure. The present model computed energy rates at stations 5 and 6 are 135.929 MW and 97.202 MW while the exergy rates are 83.915 MW and 39.9044 MW respectively. The departure in energy and exergy rates at stations 5 and 6 with those of [47] may be attributed to larger variations of the molar enthalpies and entropies together with higher values of the mole fractions of the product constituents in the overall combustion reaction compared to those obtained in the model [47]. Another cause for these deviations could also be the variation in specific heats of the constituents determined on absolute temperature terms.

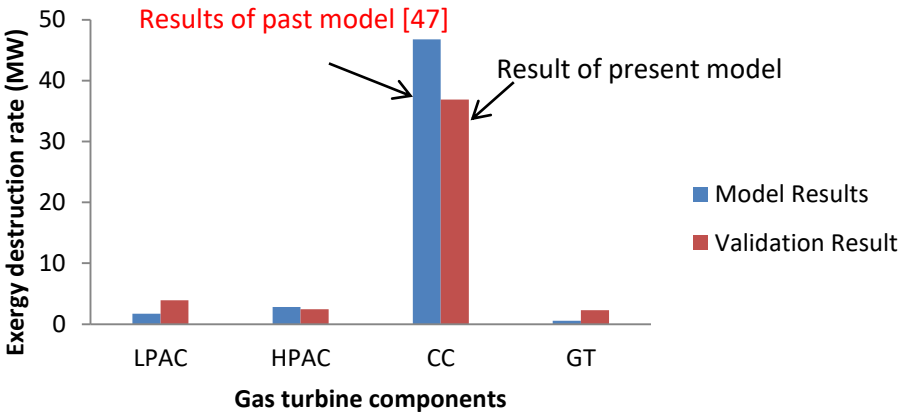

Fig.5.4. Station wise exergy destruction rates of the gas turbine in *MW*.

The comparison between the exergy destruction rates obtained from the present GT model and the model [47] is presented in Fig.5.4. Similar to the model [47], from the present model also, the gas turbine is found to have the minimum exergy destruction, and the maximum exergy destruction is found in the GT combustion chamber. It has also been observed that the present exergy destruction rates in the GT and LPAC are higher than those of [47] with the LPAC having a higher exergy destruction rate than the HPAC. Due to the deviations of energy and exergy rates at the corresponding states, the exergy destruction rates in the CC and HPAC are found to be lower than the model results of [47]. The exergy destruction rates in the GT plant components obtained from the present model are LPAC: 3.906 MW, HPAC: 2.465 MW, GTCC: 36.892 MW and GT: 2.284 MW respectively.

5.6. Summary

The exergy analysis of a combined MHD-GT power plant was performed to study the effects of ionized combustion products of MHD on the exergetic performance of the system. The analysis was carried out with the assumptions of an isentropic nozzle and the absence of pseudo-shocks on a macroscopic level. The thermodynamic properties of the partially ionized species and the un-dissociated

products in molecular forms were determined for the MHD plant. For the gas turbine plant, only the molecular properties were determined due to non-ionization of its combustion products. For the MHD an exergetic performance comparison was made between the effects of ionized species and the purely molecular species. The results of the GT were validated against proven published data analytically. The key results of the present work can be summarized as follows:

- Exergy analysis of MHD or MHD-based combined systems can provide a true picture of the inefficiencies in components closer to actual MHD operation only when the effects of ionized species are taken into account.
- When the entire MHD plant is analyzed, it shows that the exergy destruction rates and the exergetic efficiencies of the components of MHD as well as the net power output are influenced by the ionized conducting fluid from the combustor up to the generator of the MHD.
- Beyond the MHD generator, due to the decrease in temperature below the ionization temperature the exergy destructions and the exergetic efficiencies of other MHD components are independent of the influence of ionization effects and their values are based upon the flow gas properties in the molecular states.
- The exergy destruction rates in the MHD system components under the partial ionization effects can be arranged in the order of MHDCC > Generator > nozzle. Downstream of the MHD generator where the ionization effects are negligible due to low temperature, the process heater has the highest exergy destruction rate with the stack having the lowest exergy destruction.
- The nozzle in the MHD power generation unit under the ionization effect possesses the highest exergetic efficiency with 87.148 % followed by the generator of the MHD with 83.027 % and the MHD combustor with 71.036 % respectively.

- In the gas turbine, where the products are in undissociated states, the exergy destruction rate is the highest in the GT combustor with 53.923 MW, the air compressor with 3.581 MW and the turbine with 1.192 MW to follow. The order of exergetic efficiencies of the GT plant components is in the reverse order of exergy destruction. As such, the exergetic efficiency is the lowest for the GT combustor and the highest in the turbine while it is intermediate in the air compressor.
- Provided the air preheater-II is a part of MHD system, otherwise as a GT component it has the highest exergetic efficiency next to the turbine with an exergy destruction rate greater than that of the GT air compressor.
- Evaluation of exergy destruction rates and the exergetic efficiencies of MHD power generation unit up to the generator, when based on purely molecular properties, is an unrealistic approach as MHD power output and efficiency are dependent upon the degree of ionization of the conducting fluid.

Thus, the present study showed the advantages of using partial ionization in the exergy analysis of MHD power plants. The departure from the correct estimation of net power output, exergy destruction, and efficiency values of the MHD power plant can be immensely reduced by using the ionized species of combustion in the analysis and also choosing the right proportion of the ionised to non-ionized fractions of the combustion products. Further investigations of fuel mixture flammability and reacting flow momentum due to ionization behavior that may affect MHD power generation and MHD overall performance can be considered as a scope of study in the near future.

Bibliography

[1] Sustainable Development Goals. *Affordable and Clean Energy*. Retrieved on April 20, 2021 from http:// www.un.org/sustainable development/energy/.

[2] Seetharaman, A., Moorthy, M. K., Patwa, N., Saravanan., and Gupta, Y. Breaking barriers in deployment of renewable energy. *Heliyon*, 5(1):1-23, 2019. https://doi.org/10.1016/j.heliyon.2019.e01166

[3] Malghan, V. R. History of MHD power plant development. *Energy Conversion and Management*, 37 (5): 569-590, 1996.

[4] Krishnan, R. A. and Jinshah, B. S. Magnetohydrodynamics power generation. *International Journal of Scientific and Research Publications*, 3: 1-11, 2013.

[5] Retrieved on April 25, 2021, from https://www.mhdtechnologycorporation.com/

[6] Al-Habahbeh, O. M., Al-Saqqa, M., Safi, M., and Abo, K. T. Review of magnetohydrodynamic pump applications. *Alexandria Engineering Journal*, 55: 1347-1358, 2016. http://dx.doi.org/10.1016/j.aej.2016.03.0011110-0168Ó2016

[7] Farrokhi, H., Otuya, D. O., Khimchenko, A., and Dong, J. Magnetohydrodynamics in biomedical applications. *Ferro Hydrodynamics and Magneto Hydrodynamics*, *Intechopen*, pages 1-30. http://doi/10.5772/intechopen.87109

[8] Fridman, A. *Plasma Chemistry*. Cambridge University Press, New York, 1st edition, 2008.

[9] Shuler, K. and Fenn, J. Ionization in high temperature gases. *Progress in Astronautic and Aeronautics*, 12: 5-65, 1963.

[10] Mousavi, S. M., Abolfazli-E. J., and Yazdi-M. M. Numerical study of entropy generation in the flameless oxidation using large eddy simulation model and open foam software. *International Journal of Thermodynamic*, 17 (4): 202-208, 2014.

[11] Kamali, R., Mousavi, S. M., Binesh, A. R., and Abolfazli-E. J. Large eddy simulation of the flameless oxidation in the IFRF furnace with varying inlet conditions. *International Journal of Spray and Combustion Dynamics*, 9 (2): 102-115, 2017.

[12] Mousavi, S. M. and Abolfazli-E. J. Numerical investigation of the flameless oxidation of natural gas in the IFRF furnace using large eddy simulation. *International Journal of Spray and Combustion Dynamics,* 6 (4): 387-410, 2014.

[13] Mousavi, S. M., Kamali, R., Sotoudeh, F., Karimi, N., and Lee, B. J. Numerical investigation of the plasma-assisted MILD combustion of a CH_4/H_2 fuel blend under various working conditions. *Journal of Energy Resources Technology,* 143 (6): 062302-1-12, 2021.

[14] Mousavi, S. M., Kamali, R., Sotoudeh, F., Karimi, N., and Jeung, I. S. Numerical investigation of the effects of swirling hot co-flow on MILD combustion of a hydrogen–methane blend. *Journal of Energy Resources Technology,* 142 (11):112301-13, 2020.

[15] Davidson, P. A. *An Introduction to Magnetohydrodynamics***.** Cambridge University Press, UK, 2001.

[16] Demutskii, V. P. and Polovin, R. V. *Fundamentals of Magnetohydrodynamics.* Springer-Verlag, US, 1990.

[17] Alboussière, T. Fundamentals of MHD. *Les Houches*, 88: 1-44, 2008.

[18] Poonthamil, R. S., Prakash, S., and Varma, A. K. Enhancement of power generation in thermal power plant using MHD system. *IOSR Journal of Mechanical and Civil Engineering*, 13 (5): 142-146, 2016.

[19] Kayukawa, N. Open-cycle magnetohydrodynamic electrical power generation: a review and future perspectives. *Progress in Energy and Combustion Science*, 30(1): 33-60, 2004.

[20] Chernyshev, V. International co-operation in MHD electrical power generation. *IAEA Bulletin*, 20: 42-53, 1978.

[21] Rosa, R. J., Krueger, C. H., and Shioda, S. Plasma in MHD power generation. *IEEE Transactions on Plasma Science*, 19: 1180-1190, 1991.

[22] Szargut, J. Energy and exergy analysis of the preheating of combustion reactants. *Energy Research,* 12 (1): 45-58, 1988.

[23] Horn, G., Sharp, G. A., Hryniszak, W. R. Air heaters and seed recovery for M.H.D. Plant. *Philosophical Transactions of the Royal Society of London. Series A, Mathematical and Physical Sciences,* 261 (1123): 514-554, 1967.

[24] Murakami, T., Nakata, Y., Okuno, Y., and Yamasaki, H. An analytical study of the plasma conditions and performance of an MHD generator. *Electrical Engineering in Japan*, 144 (2): 9-15, 2003.

[25] Sheth, A. C., and Johnson, T. R. Evaluation of available MHD seed-regeneration processes on the basis of energy considerations. Technical Report No. ANL/MHD-78-4 TRN: 79-007777, Department of Energy/Fossil Energy MHD Division, Argonne National Laboratory, Arsonne, Illinois, U.S, 1978.

[26] Cicconardi, P. S. and Perna, A. Performance analysis of integrated systems based on MHD generators. *Energy Procedia*, 45:1305-1314, 2014.

[27] Aithal, S. M. Characteristics of optimum power extraction in a MHD generator with subsonic and supersonic inlets. *Energy Conversion and Management*, 50: 765-771, 2009.

[28] Assad, M. El. H. Thermodynamic analysis of MHD power cycle. *Mechanical Systems Engineering*, 1: 1-3, 2015.

[29] Sahin, B., Ali, K., and Hasbi, Y. A performance analysis for MHD power cycles operating at maximum power density. *Journal of Physics D. Applied Physics*, 29: 1473-1475, 1996.

[30] Ayeleso, A. O and Kahn, Md. T. E. Modelling of a combustible ionised gas in thermal power plants using MHD conversion system in South Africa. *Journal of King Saud University-Science*, 30: 367-374, 2018.

[31] Chen, L., Gong, J., Sun, F., and Wu, C. Heat transfer effect on the performance of MHD power plant. *Energy Conversion and Management*, 43(15): 2085-2095, 2002.

[32] Pattanayak, L. Thermodynamic modeling and exergy analysis of gas turbine cycle for different boundary conditions. *Power Electronics and Drive System*, 6 (2): 205-215, 2015.

[33] Bejan, A., Tsatsaronis, G., and Moran, M. J. *Thermal Design and Optimization*. John Wiley & Sons Inc., New York, 1996.

[34] Kotas, T. J. *The Exergy Method of Thermal Plant Analysis*. Exergon Publishing Company Ltd., London, UK, 2012.

[35] Tsatsaronis, G., Morosuk, T., Koch, D., and Sorgenfrei, M. Understanding the thermodynamic inefficiencies in combustion processes. *Energy*, 62: 3-11, 2013.

[36] Dincer, I. and Rosen, M. A. Exergy, Energy, Environment and Sustainable Development. Elsevier Science, UK, 2nd edition, 2013.

[37] Bejan, A. Fundamentals of exergy analysis, entropy generation minimization, and the generation of flow architecture. *Energy Research*, 26: 545-565, 2002.

[38] Mousavi, S. M., Kamali, R., Sotoudeh, F., Karimi, N., and Khojasteh, D. Large eddy simulation of pseudo shock structure in a convergent–long divergent duct. *Computers and Mathematics with Applications*, 81: 823-837, 2021.

[39] Baruah, P. K. and Baruah, M. K. Sulphur in Assam coal. *Fuel Processing Technology*, 46: 83-97, 1996.

[40] Turns, S. R. *An Introduction to Combustion Concepts and Applications*. McGraw Hill Education Private Ltd, India, 3rd edition, 2012.

[41] Bowman, C.T., Hanson, R. K., Davidson, D. F., W.C. Gardiner, W. C., Jr., V. Lissianski, G.P. Smith, D.M. Golden, M. Frenklach and M.Goldenberg, http://www.me.berkley.edu/gri_mech/

[42] Mori, Y., Ohtake, K., Yamamoto,M., and Imani, K. Thermodynamic and electrical properties of combustion gas and its plasma. *Bulletin of JSME*, 11: (44): 241-252, 1968.

[43] Eiserman, W., Johnson, P., and Conger, W. L. Estimating thermodynamic properties of coal, char, tar and ash. *Fuel Processing Technology*, 3: 39-53, 1980.

[44] Channiwala, S. A. and Parikh, P. P. A unified correlation for estimating HHV of solid, liquid and gaseous fuels. *Fuel*, 81:1051-1063, 2002.

[45] Szargut, J. Chemical exergies of the elements. *Journal of Applied Energy*, 32: 269- 286, 1989.

[46] Fitzsimons, L., Corcoran, B., Young, P., Foley, G., and Regan, F. Modelling the activity of seawater and implications for desalination exergy analyses. *In Ninth Internatonal Conference on Heat Transfer, Fluid Mechanics and Thermodynamics*, pages 1-10, Malta, 2012.

[47] Sohret, Y., Acikkalp, E., Hepbasli, A., and Karakoc, T. H. Advanced exergy analysis of an aircraft gas turbine: Splitting exergy destruction into parts. *Energy*, 90: 1219-1228, 2015.

[48] Ganesan, V. *Gas Turbines*. McGraw Hill Education, India, 2017.

[49] Gogoi, T. K. and Gautam, U. Performance evaluation of a gas and steam turbine based cogeneration plant: a case study. In *Proceedings of the ASME Gas Turbine India Conference, GTINDIA2019*, pages 1 – 15, Chennai, 2019.